

Broadband ‘spectro-temporal’ features of extragalactic black hole binaries LMC X-1 and LMC X-3: An *AstroSat* perspective

Bhuvana G. R.¹★, Radhika D.¹, V. K. Agrawal², Samir Mandal³ and Anuj Nandi²

¹*Department of Physics, Dayananda Sagar University, Hosur Main Road, Bengaluru, 560068, India.*

²*Space Astronomy Group, ISITE Campus, U. R. Rao Satellite Center, Outer Ring Road, Marathahalli, Bengaluru, 560037, India.*

³*Department of Earth and Space sciences, Indian Institute of Space Science and Technology, Valiamala, Thiruvananthapuram, 695547, India.*

Accepted XXX. Received YYY; in original form ZZZ

ABSTRACT

We present the first results of extragalactic black hole X-ray binaries LMC X-1 and LMC X-3 using all the archival and legacy observations by *AstroSat* during the period of 2016 – 2020. Broadband energy spectra (0.5–20 keV) of both sources obtained from the *SXT* and *LAXPC* onboard *AstroSat* are characterized by strong thermal disc blackbody component ($kT_{in} \sim 1$ keV, $f_{disc} > 79\%$) along with a steep power-law ($\Gamma \sim 2.4 - 3.2$). Bolometric luminosity of LMC X-1 varies from 7 – 10% of Eddington luminosity (L_{Edd}) and for LMC X-3 is in the range 7 – 13% of L_{Edd} . We study the long-term variation of light curve using *MAXI* data and find the fractional variance to be $\sim 25\%$ for LMC X-1 and $\sim 53\%$ for LMC X-3. We examine the temporal properties of both sources and obtain fractional rms variability of PDS in the frequency range 0.002 – 10 Hz to be $\sim 9\% - 17\%$ for LMC X-1, and $\sim 7\% - 11\%$ for LMC X-3. The ‘spectro-temporal’ properties indicate both sources are in thermally dominated soft state. By modelling the spectra with relativistic accretion disc model, we determine the mass of LMC X-1 and LMC X-3 in the range 7.64 – 10.00 M_{\odot} and 5.35 – 6.22 M_{\odot} respectively. We also constrain the spin of LMC X-1 to be in the range 0.82 – 0.92 and that of LMC X-3 in 0.22 – 0.41 with 90% confidence. We discuss the implications of our results in the context of accretion dynamics around the black hole binaries and compare it with the previous findings of both sources.

Key words: X-ray binaries – accretion, accretion discs – black hole physics – stars: black holes – radiation mechanisms: general – stars: individual: LMC X-1 – stars: individual: LMC X-3

1 INTRODUCTION

Black Hole X-ray Binaries (BH-XRBs) consist of a black hole (BH) along with a normal companion star which are gravitationally bound to each other. Highly compact BH accretes matter from the companion star and forms an accretion disc around it. The accretion disc gets heated up due to the geometrical compression in the accretion process and gives out energy in different wavebands, mainly in X-rays. Based on the type of X-ray emission, XRBs are classified either as persistent sources or as transients (Chen et al. 1997; Tetarenko et al. 2016; Corral-Santana et al. 2016). Persistent sources are the ones that radiate X-ray luminosity consistently for a long period of time (Tanaka & Shibazaki 1996). Transients, on the other hand, undergo outburst emitting large X-ray flux (Tsunemi et al. 1989) once in a while. Generally, XRBs exist either in a low mass X-ray binary (LMXB) system or high mass X-ray binary (HMXB) system (Remillard & McClintock 2006) depending on the mass of the com-

panion star. Most of the observed transient sources typically exist in LMXBs whereas persistent sources are found in HMXBs.

To study the accretion dynamics around the black holes, it is necessary to understand the X-ray spectrum of the source. The radiation spectrum of BH-XRBs generally consists of thermal and non-thermal components. While thermal radiation comes from different radii of accretion disc (Shakura & Sunyaev 1973), non-thermal emission is due to the Comptonization of photons from the disc by hot corona (Tanaka & Lewin 1995; Chakrabarti & Titarchuk 1995). Thermal radiation from the disc forms the low energy soft X-ray flux in the energy spectra and non-thermal radiation contributes to the high energy. The emitted radiation varies with respect to energy and time, resulting in different spectral states. These spectral states are usually classified as low/hard state (LHS), hard-intermediate state (HIMS), soft-intermediate state (SIMS) and high/soft state (HSS) (Homan et al. 2001; Belloni 2005; Remillard & McClintock 2006; Nandi et al. 2012; Radhika & Nandi 2014; Radhika et al. 2016b; Nandi et al. 2018; Sreehari et al. 2019; Baby et al. 2020; Katoch et al. 2020 (under review) and references therein). Persistent BH-XRBs mainly ex-

★ E-mail: bhuvanahebbbar@gmail.com

hibit HSS and LHS (Shapiro 1973; McClintock & Remillard 1986; Main et al. 1999; Zdziarski et al. 2002; Remillard & McClintock 2006). During HSS, the X-ray energy spectrum of the source consists of a strong disc component and a weak power-law component. While the source is in LHS, the spectrum consists of a hard power-law component (Chakrabarti & Titarchuk 1995; Tanaka & Lewin 1995; Chen & Taam 1996; Haardt et al. 2001; Zdziarski et al. 2002; Nandi et al. 2012; Sreehari et al. 2018; Aneeha et al. 2019).

In addition to the spectral variability exhibited at different states, BH-XRBs show timing variability. This variability can be understood by studying the source light curve and Power Density Spectrum (PDS) which allows us to investigate the variation in power at different frequencies. During LHS, the PDS can be described by a flat-top noise with a broken power-law, and sometimes have signatures of Quasi-periodic Oscillations (QPOs) (Casella et al. 2005; Remillard & McClintock 2006; Belloni et al. 2011). PDS during HSS is characterized by a weak power-law component. Narrow frequency features are rarely seen during this state. The fractional rms amplitude in the source light curve is seen to be high ($> 10\%$) during LHS (Belloni & Hasinger 1990; Tanaka & Lewin 1995; Nowak 1995; Nandi et al. 2012) and it decreases ($< 10\%$) as the source moves towards the HSS.

During HSS, the inner edge of the disc moves towards the BH and it is predicted to be very close to the radius of innermost stable circular orbit i.e. ISCO (Shapiro & Teukolsky 1983). Most of the thermal emission during this state comes from the innermost region of the disc where there is a strong gravitational effect and these soft X-rays gives us information on specific angular momentum of the BH. Angular momentum of the BH can be expressed in terms of a dimensionless parameter called spin as $a = cJ/GM_{BH}^2$ whose magnitude varies between 0 and 1 (Zhang et al. 1997a; Shafee et al. 2006; McClintock et al. 2006, 2014). Here, J represents the angular momentum, c is the speed of light, G is gravitational constant and M_{BH} is mass of the BH. Thus by studying the disc component during thermal dominated spectra of a BH, J can be calculated which in turn gives the spin parameter if M_{BH} is known. This method of determining the spin of BH by modelling the broadband energy spectrum is known as the continuum-fitting method (Zhang et al. 1997b; McClintock et al. 2011; Steiner et al. 2014).

LMC X-1 is the first extragalactic X-ray source found in the Large Magellanic Cloud (LMC) (Mark et al. 1969). The system is a HMXB containing an O7 III star along with a black hole, which are orbiting with a period of ~ 3.9 days (Cowley et al. 1995). The mass of black hole, inclination angle of the system and distance to the source are estimated to be $10.91 \pm 1.41 M_{\odot}$, $36.38 \pm 1.92^{\circ}$ and 48.1 ± 2.22 kpc respectively (Orosz et al. 2009). Continuum fitting of energy spectra during the thermal dominated states has shown that it is a rapidly spinning black hole (see also Tripathi et al. 2020) with spin parameter $a = 0.92^{+0.05}_{-0.07}$ (Gou et al. 2009). The X-ray energy spectrum of the source is always found to be in thermal dominated state (Ebisawa et al. 1989, 1993; Schmidtke et al. 1999) with a power-law tail component above 10 keV. X-ray flux of the source is moderately variable in short period (< 1 ks) (Nowak et al. 2001) whereas very stable on long time-scale (Orosz et al. 2009). The temporal properties of LMC X-1 are similar to that of typical HSS with its PDS approximately following a power-law ($\propto \nu^{-1}$). QPOs of frequency $\sim 26 - 29$ mHz have been reported earlier and seems to be peculiar since such type of QPOs are usually found in hard state (Alam et al. 2014).

LMC X-3 is another persistent, bright, X-ray source in LMC consisting of a Roche lobe filling HMXB (Orosz et al. 2014) with a BH of mass $6.98 \pm 0.56 M_{\odot}$ (Soria et al. 2001; Orosz et al.

2014). Studies done on this object show that LMC X-3 is spinning at a very low rate with $a = 0.25^{+0.20}_{-0.29}$ (Steiner et al. 2010) and the disc inclination angle is $69.24 \pm 0.72^{\circ}$ (Orosz et al. 2014). The source is mostly found in thermal dominated state (Nowak et al. 2001) with the occasional transition to LHS (Boyd et al. 2000; Wilms et al. 2001; Smale & Boyd 2012). LMC X-3 is also found to have undergone an Anomalous Low/Hard State (ALS) repeatedly where the X-ray flux drops to a very low value ($\sim 1 \times 10^{35}$ erg/s) in lower energy (Torpin et al. 2017). The long term variability of the source has a high amplitude of the factor of ~ 4 on a 100 – 200 day time scale (Cowley et al. 1991). However, the variability in the short term scale is very less of only a few percentages (Nowak et al. 2001). Temporal studies done on the source show that the LHS consists of a strong broadband variability with fractional rms of $\sim 40\%$ along with a QPO at 0.4 Hz (Boyd et al. 2000) and HSS has less variability with no QPOs (Trevés et al. 1988). Despite having large flux variation in long term scale, the inner disc radius is found to remain constant over a long period of time (Steiner et al. 2010).

In this work, we present the first results of the broadband spectral and temporal study of the extragalactic BH-XRBs LMC X-1 and LMC X-3 carried out using all the *AstroSat* (Agrawal 2001) archival and legacy observations. *AstroSat* with its unprecedented spectral and timing resolution along with its broadband coverage forms an excellent observatory to carry out studies on XRBs. Therefore in this study, we make use of the remarkable characteristics of *AstroSat* to perform the spectral and temporal studies of the sources. Source properties during different epochs which are separated by a time gap of a few months spanning over ~ 4.5 years of the *AstroSat* era are explored. We look into the evolution of the source light curve on long term and short term in order to understand the evolution of fractional variance. While long term variability of the source light curve is studied using *MAXI* data, *LAXPC* observations are used to study the short term variability. We also investigate the nature of the PDS to estimate the fractional rms amplitude and look for the presence of any QPOs by means of temporal analysis. Further, we attempt to constrain the BH mass, spin and accretion rate by applying the relativistic disc model to the broadband energy spectra using continuum fitting method.

This paper is organized as follows. In section 2, we present the observation and data reduction method of *AstroSat* data. In section 3, we discuss the methods of timing analysis and spectral modeling. The results of temporal properties, spectral properties along with the estimation of physical parameters are presented in section 4. Finally in section 5, we discuss and conclude the results of our study of LMC X-1 and LMC X-3 using *AstroSat* observations.

2 OBSERVATION AND DATA REDUCTION

Persistent X-ray binaries LMC X-1 and LMC X-3 are observed by *AstroSat* during the period of 2016–2020 with its X-ray instruments *Soft X-ray Telescope (SXT)* (Singh et al. 2017) and *Large Area X-ray Proportional Counter (LAXPC)* (Yadav et al. 2016; Antia et al. 2017) in the energy range 0.3 – 8 keV and 3 – 80 keV respectively. We make use of its broadband energy coverage and excellent timing resolution (10 μ s) of *LAXPC* instrument in our study. We obtain all the archival and legacy observation data of these sources from the *AstroSat*-Indian Space Science Data Centre (ISSDC)¹ (see Table

¹ https://astrobrowse.issdc.gov.in/astro_archive/archive/Home.jsp

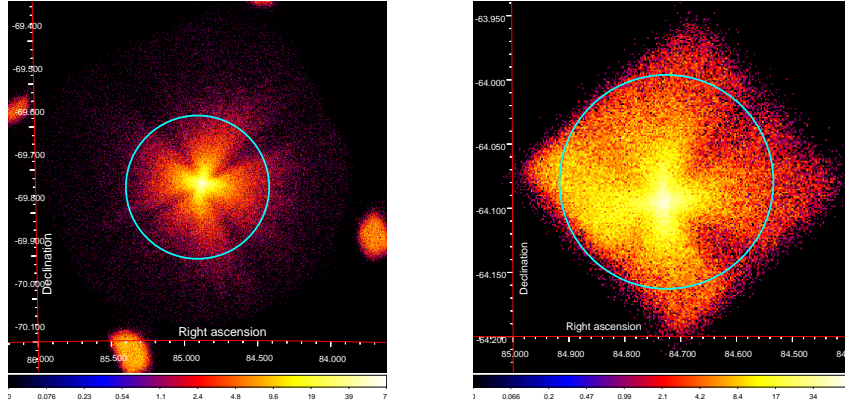


Figure 1. *AstroSat* - *SXT* images of the sources LMC X-1 and LMC X-3 obtained using PC and FW modes are shown respectively in the left and right panels. These two images represent observations during MJD 57717 and MJD 58155 respectively. We consider a circular region of $10'$ for LMC X-1 and $5'$ for LMC X-3 as marked in the images from which the spectrum and light curve are extracted (see section 2.1 for details). The bright spots in the corner of PC mode image are from the calibration sources.

Table 1. The log of LMC X-1 and LMC X-3 observations by *AstroSat*.

LMC X-1			
Observation Id	Date (MJD)	Epoch	Exposure (s)
A02_118T01_9000000826	57717	1	62210
A03_119T02_9000001496	57993	2	14554
A08_008T01_9000003414	58854	3	62074
A08_008T01_9000003596	58939	4	4573
A08_008T01_9000003596	58940	5	53504
LMC X-3			
Observation Id	Date (MJD)	Epoch	Exposure (s)
G05_212T01_9000000600	57614	1	25712
G05_212T01_9000000672	57650	2	21423
A03_106T01_9000001130	57846	3	19408
A03_106T01_9000001190	57862	4	28600
A04_112T01_9000001698	58074	5	28905
A04_112T01_9000001778	58104	6	42962
A04_112T01_9000001884	58155	7	32550
A04_112T01_9000001908	58169	8	32738
A08_008T02_9000003430	58860	9	56862

1). We also make use of *MAXI* data obtained from “*MAXI/GSC* on-demand web interface”² to plot the long term light curve and hardness ratio.

2.1 *SXT* Data Reduction

X-ray imaging instrument *SXT* operates in the energy range of 0.3 – 8 keV. For the analysis of *SXT* data, we follow the guidelines provided by *SXT* team³ (see also Sreehari et al. 2019; Baby et al. 2020 for details). *SXT* has observed both sources LMC X-1 and LMC X-3 in Photon Counting (PC) mode and some of the LMC X-3 observations in Fast Window (FW) mode. Level-2 *SXT* data for all the observations are obtained from the ISSDC data archive. Individual orbit data are merged into a single event file with the *SXT* event merger tool using *Julia v1.1*. The resultant cleaned event file is used to extract the spectrum and light curve in 0.3 – 8 keV energy

range using *XSELECT v2.5g*. *SXT* image of the source has count rate < 40 counts/s and we did not find any effect of pile-up (following the criteria given in *AstroSat* handbook⁴). Therefore, a circular region of radius $10'$ (left panel of Figure 1) and $5'$ (right panel of Figure 1) are chosen for PC and FW modes respectively. From this region, the spectrum and light curve for further analysis are extracted. *SXT* background file and response matrix file (rmf) provided by the *SXT* instrument team are used. The auxiliary response file (ARF) for the selected source extraction region is obtained using *sxtarfmodule*. In the energy spectrum, data is grouped with 20 counts in a single bin. A gain fit correction is applied for *SXT* spectrum using the *gain fit* command to account for instrumental features at low energy values of 1.8 keV and 2.2 – 2.4 keV for absorption edges of Si & Au respectively (see also Singh et al. 2017 and *SWIFT-XRT* website⁵).

2.2 *LAXPC* Data Reduction

LAXPC Level-1 data is downloaded from the ISSDC data archive. Level-1 data is processed to Level-2 by using the *LAXPC* pipeline software (*LaxpcSoft*⁶). We make use of the data from *LAXPC 20* only for the uniform study of observations during 2016–2020, due to gain instability reported in *LAXPC 10* and *LAXPC 30* detectors⁷ (see also Baby et al. 2020). Observation specific response and background files generated by the software following Antia et al. 2017 are used. The software routine creates the Good Time Interval (GTI) file consisting of timing information during Earth occultation and South Atlantic Anomaly (SAA). *LAXPC* data is obtained by considering the single events and top layer of the detector unit (see also Sreehari et al. 2019; Katoch et al. 2020 (under review)). The analysis and modelling methods of the reduced data are presented in the next section.

⁴ <https://www.issdc.gov.in/docs/as1/AstroSat-Handbook-v1.10.pdf>

⁵ https://www.swift.ac.uk/analysis/xrt/digest_cal.php#res

⁶ https://www.tifr.res.in/~astrosat_laxpc/LaxpcSoft.html

⁷ <http://astrosat-ssc.iucaa.in/>

² <http://maxi.riken.jp/mxondem/>

³ http://www.tifr.res.in/~astrosat_sxt/dataanalysis.html

3 ANALYSIS AND MODELLING

3.1 Temporal Analysis

Source light curves with a time-bin of 1 day, obtained from *MAXI* observations⁸ in the energy range of 2 – 20 keV, 2 – 6 keV and 6 – 20 keV are used to study the long term variance of the sources. The hardness ratio (HR) is obtained by dividing the source flux (in units of photons/cm²/s) of the two light curves (i.e. flux of 6 – 20/2 – 6 keV). We estimate the fractional variance of the light curve for the period of 2016 – 2020 using $F_{var} = \left(\sqrt{S^2 - \sigma_{err}^2} \right) / \bar{x}$ following [Vaughan et al. 2003](#). Here, S^2 is the total variance of the light curve and σ_{err}^2 is the error associated with measurement and \bar{x} is the mean count rate of the light curve.

We generate the *LAXPC* light curves with 1 sec time-bin to study the short term variability of the sources in the energy range of 3 – 20 keV. *LAXPC* light curves of 50 ms time-bin in the energy range of 3 – 20 keV are also considered to study the nature of the PDS. Each light curve is divided into intervals of 8192 time bins and the PDS is constructed for each of these bins. The average of these PDS is obtained and is binned logarithmically by a factor of 1.05 in the frequency space. The resultant binned PDS are normalized to get the fractional rms spectra ([Belloni & Hasinger 1990](#)) and the Poisson noise is subtracted implementing the procedure mentioned by [Agrawal et al. 2018](#). The resultant PDS in the frequency range 0.002 – 10 Hz is fitted with a *powerlaw* distribution function in the form of $P(\nu) = A\nu^\gamma$, where γ is the power-law index and A is the norm.

We also estimate the fractional rms amplitude in the frequency range 0.002 – 10 Hz using the rectangle rule integration method given by $rms = \sqrt{(P \times \Delta\nu)} \times 100$ (in %)⁹ (see also [Radhika et al. 2016a,b, 2018](#) for details), where P is the power in the units of rms²/Hz and $\Delta\nu$ is the frequency in Hz. We follow the above mentioned procedures for both sources and obtained timing results are presented in section 4.1.

3.2 Spectral Analysis

As the energy spectra of both sources have no significant flux above 20 keV, we consider the *SXT* spectrum in the energy range of 0.5 – 7 keV and that of *LAXPC* in 4 – 20 keV. Broadband energy spectra (0.5–20 keV) are analyzed and modeled using *XSpec v12.10* tool ([Arnaud 1996](#)) of *HEASOFT v6.26.1*.

We use *TBabs* model to represent the hydrogen column density (n_H) along the line of sight. Since much of the absorption of X-ray from LMC X-1 and LMC X-3 is due to the metallic abundance in the host galaxy ([Hanke et al. 2010](#)), we consider the LMC abundance following [Hanke et al. \(2010\)](#) in our calculation of n_H . These abundance values are adapted by using the *abund file* command in *XSpec* during the spectral fit. Initially, we model the broadband spectral data using a single *powerlaw* along with an absorption model by keeping the parameters of *powerlaw* in both data set independent of each other. It is observed that the unfolded spectrum with respect to *powerlaw* along-with the ratio of data by *powerlaw* model shows instrumental smearing ([Vaughan et al. 1999](#); [Boller et al. 2002](#); [Fabian et al. 2002](#); [Fabian & Vaughan 2003](#)) as well as the

need for disc component in the lower energy range. Then, in order to study the spectral properties of the source, we model the broadband (0.5 – 20 keV) energy spectrum of LMC X-1 for all the epochs with the phenomenological model *TBabs(diskbb+powerlaw)*. This model combination is referred as Model-1. An overall systematic error of 1% is incorporated into all the fits to account for uncertainty in the response matrix. For LMC X-3, energy spectra of all the epochs are found to be very soft with significant data till 10 keV. Therefore, we use Model-1 for spectral modeling of LMC X-3 without *powerlaw* component for all observations except Epochs 1 and 4. However, a *smedge* is included to account for the reflection seen above 7 keV for most of the epochs. We also made an attempt to model the spectra with physical model *nthcomp* ([Zycki et al. 1999](#)) of *XSpec* but the fit did not give meaningful physical parameter values and χ^2_{red} obtained was > 2 . From the broadband energy spectra, we calculate the unabsorbed bolometric source flux (in 0.1 – 100 keV) as well contribution of disc flux (in 0.5 – 20 keV) over the total unabsorbed flux using the *cflux* model. The hardness ratio (HR) is calculated by estimating the ratio of flux in the energy range 6 – 20 keV and 3 – 6 keV. Errors for all the parameters are obtained at 90% confidence interval, and relevant error propagation formulae are also implemented based on [Bevington & Robinson 2003](#).

Further, we model the broadband energy spectra using several relativistic accretion disc models in order to constrain the physical parameters of the BHs. In this regard, we consider the *kerrbb* model ([Li et al. 2005](#)), which assumes a thin, relativistic accretion disc around a Kerr black holes. Therefore, we model the broadband energy spectra using the continuum model combination of *kerrbb* and *simpl* ([Steiner et al. 2009](#)) in order to constrain the mass (M_{BH}), spin (a) and mass accretion rate (\dot{M}) of the system. We refer to the model combination: *TBabs(kerrbb*simpl)* as Model-2 hereafter. While *kerrbb* takes into account of the relativistic effect on soft X-ray from the accretion disc, *simpl* model considers the Comptonization process of the disc photons. While using Model-2 for both sources, we consider the known values of inclination angle and distance (see section 1). The detailed results obtained from timing and spectral modeling are presented in section 4.

4 RESULTS

4.1 Temporal Properties

In this section, we present the temporal properties and lightcurve variability of LMC X-1 and LMC X-3 using *LAXPC* data. Along with this, we present the long-term light curve variability of the sources as observed by *MAXI* for a period of ~ 4.5 years (MJD 57400 - MJD 59000) within the duration of *AstroSat* observations. In the left side of Figure 2, we show the variability of the light curve in 2 – 6 keV (top panel), 6 – 20 keV (middle panel) and HR (bottom panel) of LMC X-1. In the right side of Figure 2, we plot the same for LMC X-3. It is observed that LMC X-1 does not show significant variability and the average HR of this source is ~ 0.2 . The fractional variance F_{var} of the light curve in the energy range 2 – 20 keV, is calculated using the method mentioned in section 3.1 is found to be 24.9% for LMC X-1. On the other hand, LMC X-3 shows significant intensity variation with HR in the range 0.01 – 2.0. The F_{var} calculated for LMC X-3 considering the entire time period is found to be 52.9%. The light curve periodicity during the initial 700 days is $\sim 100 - 200$ days and beyond that, the source has a random variability pattern (see top right panel of Figure 2 for LMC X-3). Short term variability of the source is studied using *LAXPC* light

⁸ <http://maxi.riken.jp/mxondem/>

⁹ https://heasarc.gsfc.nasa.gov/docs/xte/recipes/pca_fourier.html

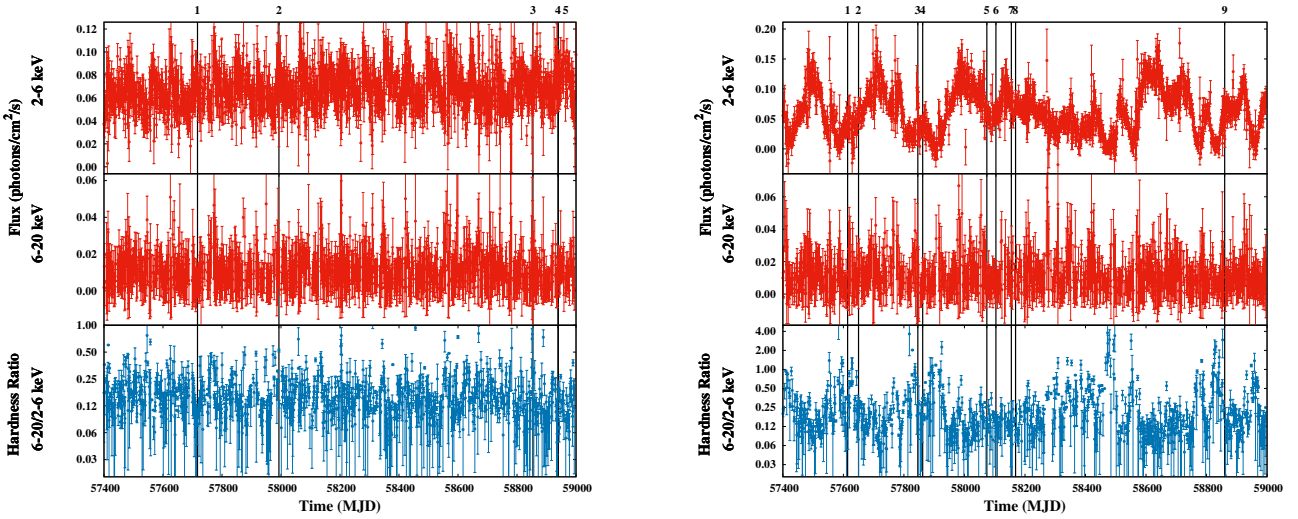


Figure 2. *MAXI* light-curve of LMC X-1 (left panel) and LMC X-3 (right panel) during the period of 2016 – 2020 in the energy band of 2 – 6 keV (top panel) and 6 – 20 keV (middle pane). Ratio of the flux in hard energy and soft energy bands (6 – 20/2 – 6 keV) is plotted in bottom panel. All the *AstroSat* observations considered for these sources have been marked in black vertical lines along-with corresponding Epoch numbers.

curve. It is found that the average source intensity for LMC X-1 varies in the range of 39 – 52 counts/sec (3 – 20 keV) and HR in 0.10 – 0.33 between different epochs. In the case of LMC X-3, the source count rate in different observations varies between 50 – 240 counts/sec (3 – 20 keV) and HR is in the range 0.07 – 0.21. The fractional variance of light curve is estimated to be varying in the range of 7.41% – 15.89% and 9.7% – 23.9% during the different epochs of LMC X-1 and LMC X-3 respectively.

As mentioned in section 3.1, we obtain the power spectrum for each observation of both sources in the frequency range of 0.002 – 10 Hz using *LAXPC* lightcurve with 50 msec binning. We model the PDS using *powerlaw* model for all observations of LMC X-1 (shown for epochs 1, 2 and 4 in the left panel of Figure 3). No narrow frequency signatures are seen in the PDS. The fractional rms amplitude in the frequency range 0.002 – 10 Hz estimated to be varying from 9.86% to 16.7% during the different epochs. Similarly, PDS for all observations of LMC X-3 are fitted using *powerlaw* model. Fitted PDS corresponding to four epochs are shown in the right panel of Figure 3. None of the PDS show any narrow frequency signature. The fractional rms amplitude of the PDS is in the range of 7.16 – 10.9%. In Table 2, we present estimated parameters from the temporal study for both sources.

4.2 Spectral Properties

4.2.1 LMC X-1

AstroSat has observed the source LMC X-1 during five epochs (see Table 1) with a time gap of several months. From the spectral fit, we get the n_H value of $1.22 \pm 0.02 - 1.48 \pm 0.04 \times 10^{22}$ during different epochs. These values are greater than that obtained using only the Galactic abundance (Wilms et al. 2000) which is $\sim 0.6 \times 10^{22}$ atoms cm^{-2} . We note that the Epoch-1 spectrum requires an additional cut-off at $6.29^{+0.08}_{-0.09}$ keV which is taken into account with a *highecut* model (χ^2_{red} improves from 1.94 to 1.32). During the different epochs, the value of disc temperature (T_{in}) varies from $0.86 \pm 0.01 - 0.98 \pm 0.01$ keV, while the photon index (Γ) is in the range $2.46 \pm 0.04 - 3.29 \pm 0.04$. The bolometric luminosity calculated (0.1 – 100 keV) is in the range of 8.4×10^{37} erg/s ($\equiv 0.07$

L_{Edd}) to 1.17×10^{38} erg/s ($\equiv 0.10 L_{Edd}$). Total flux is found to be contributed mainly from the disc with 79% - 94% contribution. Also, the value of the hardness ratio is observed to vary from 0.16 to 0.34. We do not observe any feature of Fe line emission in any of the epochs, but a reflection edge exists > 7 keV during Epochs 1 and 2. The folded spectrum of Epoch-4 of LMC X-1 is shown in the left plot of Figure 4. In Table 3, we summarize the values obtained for the parameters using Model-1.

The observed inner disc radius of the accretion disc r_{in} is calculated using the normalization (N_{diskbb}) value of *diskbb*. N_{diskbb} and disc radius are related as $N_{diskbb} = (r_{in}/D_{10})^2 \times \cos \theta$, where r_{in} is the observed inner disc radius, D_{10} is the distance to the source in 10 kpc and θ is the inclination angle of the disc. However, since r_{in} is the apparent radius we estimate the ‘true’ radius following Kubota et al. 1998. ‘True’ radius is given as $R_{in} = \xi \cdot \kappa^2 \cdot r_{in}$ where κ is taken to be 1.55 (see section 4.3 for details) and $\xi = 0.412$ as given by Kubota et al. 1998. We obtain the value of ‘true’ radius R_{in} to be varying from 29.65 ± 0.71 km to 39.17 ± 0.71 km during the different epochs of LMC X-1.

4.2.2 LMC X-3

LMC X-3 has been observed by *AstroSat* during nine epochs with a time gap of several months (see Table 1). The n_H value obtained during different epochs is in the range of $0.03 \pm 0.01 - 0.07 \pm 0.02 \times 10^{22}$ atoms cm^{-2} . Its average value is slightly higher than that obtained by considering only the Galactic abundance ($\sim 0.04 \times 10^{22}$ atoms cm^{-2}). During the different epochs, the value of disc temperature is ~ 1 keV while the norm varies from $16.18^{+0.97}_{-0.90}$ to $21.35^{+1.30}_{-1.72}$. No Fe line features are observed in any of the spectra. Unabsorbed bolometric luminosity (0.1 – 100 keV) is found to vary between $5.10 \times 10^{37} - 1.02 \times 10^{38}$ erg/s ($\equiv 0.07 - 0.13 L_{Edd}$). The disc flux contribution and hardness ratio calculated are $> 96\%$ and 0.10 – 0.19 respectively throughout the different observational epochs. Modified inner disc radius R_{in} is found to be in the range $32.40 \pm 0.95 - 37.21 \pm 0.95$ km, considering $\kappa = 1.7$. We plot the folded spectrum of Epoch-5 data of LMC X-3 in Figure 4. The spectral parameters of best-fit values are mentioned in Table 3.

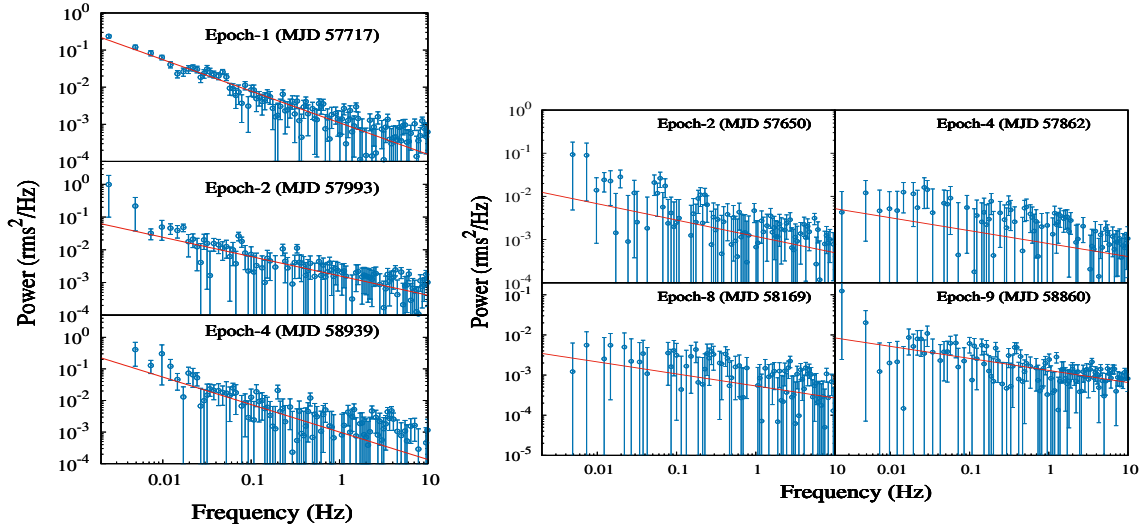


Figure 3. Power spectra of both sources (LMC X-1 in left panel and LMC X-3 in right panel) during different observations in the frequency range of 0.002 – 10 Hz. The PDS are modeled with different *powerlaw* components whose values are quoted in Table 2. See text for details.

Table 2. Details of results obtained for temporal analysis of the sources LMC X-1 and LMC X-3. The PDS corresponds to frequency range of 0.002 – 10 Hz in the energy band 3 – 20 keV. *powerlaw* model is used to fit the PDS with power-law index γ and norm n_{PL} . Fractional rms amplitude value calculated is given in %. We also quote the fractional variance F_{var} , estimated for variability of *LAXPC* light curve which is discussed in section 4.1. Errors are calculated with 90% confidence for all the parameters.

LMC X-1					
Epoch	γ	n_{PL}^{\dagger} (in units of 10^{-3})	fractional rms (%)	χ^2/dof	F_{var} (%)
1	-0.85 ± 0.04	1.10	10.14	125.9/109 = 1.15	11.9
2	-0.59 ± 0.09	1.59	12.1	122.1/109 = 1.12	13.14
3	-0.65 ± 0.04	1.15	8.99	88.30/109 = 0.81	7.41
4	$-0.87^{+0.16}_{-0.22}$	1.01	16.7	105.8/109 = 0.97	15.89
5	-0.83 ± 0.03	1.23	9.86	117.1/109 = 1.09	11.18
LMC X-3					
1	-0.20*	1.15	8.37	141.7/108 = 1.31	9.7
2	-0.37 ± 0.09	1.18	10.8	115.5/109 = 1.08	16.1
3	$-0.72^{+0.25}_{-0.16}$	0.83	10.9	122.0/108 = 1.13	19.0
4	-0.3*	1.20	8.8	115.2/109 = 1.06	23.9
5	$-0.25^{+0.14}_{-0.20}$	1.12	9.9	117.2/108 = 1.08	14.7
6	-0.2*	0.60	7.16	99.4/109 = 0.91	12.3
7	-0.3*	0.66	7.6	113.9/109 = 1.04	11.5
8	-0.3*	0.59	7.09	127.4/109 = 1.17	17.4
9	$-0.14^{+0.09}_{-0.08}$	1.00	10.3	110.5/109 = 1.01	11.9

* Frozen

† The error values are trivial and hence not quoted.

4.3 Constraining the physical parameters of the black hole

We understand from sections 4.2.1 and 4.2.2 that both sources have a soft energy spectrum dominated by the contribution from the disc component flux. Hence we attempt to estimate the source mass and spin using the broadband continuum fitting method. For this purpose, we model the spectra with Model-2.

The important model parameters obtained are \dot{M} , a , M_{BH} in units of M_{\odot} , photon index (Γ) and scattering fraction (*FracScat*). We estimate \dot{M} of LMC X-1 to be of $1.24^{+0.10}_{-0.11} - 2.16^{+0.39}_{-0.17} \times 10^{18}$ g/s. We find that this value of accretion rate is 0.29 – 0.51 of the Eddington rate (M_{Edd}). Gou et al. 2009 estimated the spectral hardening factor for this source to be 1.55 using *RXTE* observations during which the source existed in a thermal dominated state. Since all the *AstroSat* observations considered in this paper also have

thermal disc dominated spectra with almost constant luminosity, we choose the same value for the hardening factor. To confirm the consistency of this value, we fit the spectral data by keeping hardening factor as a free parameter, which resulted in a value of 1.54 – 1.56 for different epochs. Hence, we consider the hardening factor to be 1.55 for all the epochs of LMC X-1. We note that the resultant parameters using the *simpl* model i.e. Γ is $\sim 2.61^{+0.15}_{-0.19} - 4.50^{+0.03}_{-1.28}$ and the *FracScat* is in the range $0.03^{+0.03}_{-0.01} - 0.2^{+0.03}_{-0.02}$ for different epochs of LMC X-1. The \dot{M} of LMC X-3 is in the range $2.02^{+0.09}_{-0.06}$ to $4.03^{+0.17}_{-0.14} \times 10^{18}$ g/s which corresponds to 0.14 – 0.29 of M_{Edd} . Spectral hardening factor of 1.7 is considered for these fits of LMC X-3.

We obtain the source mass for LMC X-1 to be in the range of $7.64^{+0.99}_{-0.25} M_{\odot}$ to $10.00^{+0.52}_{-1.22} M_{\odot}$ during the different epochs. The

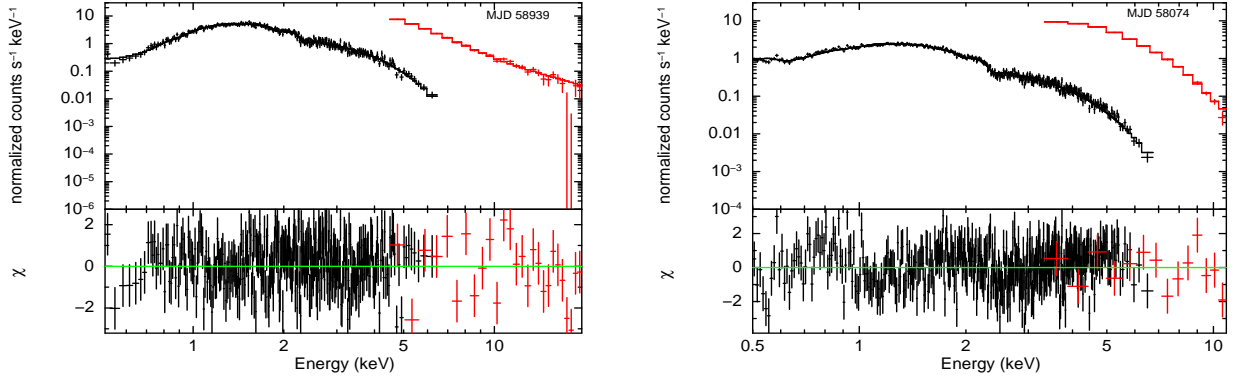


Figure 4. Broadband spectral fitting performed for Epoch-4 observation of LMC X-1 (left) in 0.5 – 20 keV and Epoch-5 observation of LMC X-3 (right) in 0.5 – 10 keV. Combined *SXT* and *LAXPC* spectrum is modelled with Model-1 for LMC X-1 and *diskbb* along with *smedge* for LMC X-3.

Table 3. Spectral parameter values obtained from the best-fit of Model-1 for both LMC X-1 and LMC X-3. T_{in} (in units of keV) corresponds to disc temperature, N_{diskbb} is disc norm. The parameters of *powerlaw* are denoted by the photon index Γ and norm N_{PL} . The value of *edgeE* is the energy component from the *smedge* model. L_{bol} is the bolometric luminosity for the energy range 0.1 – 100 keV in units of 10^{38} erg/s estimated by incorporating the known values of mass quoted in section 1. f_{disc} and f_{total} are unabsorbed disc flux and total flux calculated in the energy range 0.5 – 20 keV. *HR* corresponds to the hardness ratio estimated for ratio of flux in 6 – 20 keV and 3 – 6 keV. Error for all the parameters are calculated with 90% confidence, and by also considering the error propagation method wherever appropriate.

LMC X-1									
Epoch	T_{in} (keV)	N_{diskbb}	Γ	N_{PL}	<i>edgeE</i> (keV)	L_{bol} ($\times 10^{38}$ erg/s)	f_{disc}/f_{total} (%)	<i>HR</i>	χ^2/dof
1*	0.86 ± 0.01	$53.41^{+3.15}_{-3.09}$	2.63 ± 0.02	0.10^{\ddagger}	$7.54^{+0.87}_{-0.70}$	0.94	84	0.21 ± 0.02	$700.39/529 = 1.32$
2	$0.90^{+0.02}_{-0.01}$	$46.17^{+4.86}_{-4.35}$	2.46 ± 0.04	0.16 ± 0.01	$8.28^{+0.36}_{-0.35}$	1.17	82	0.34 ± 0.02	$582.95/417 = 1.39$
3	0.96 ± 0.01	$35.02^{+1.77}_{-1.77}$	3.29 ± 0.04	0.10^{\ddagger}	-	0.84	86	0.16 ± 0.02	$670.77/506 = 1.32$
4	0.98 ± 0.02	$30.96^{+1.77}_{-0.91}$	$3.03^{+0.13}_{-0.16}$	0.09^{\ddagger}	-	1.02	79	0.24 ± 0.03	$393.08/338 = 1.16$
5	0.98 ± 0.01	$30.74^{+0.29}_{-0.17}$	$3.19^{+0.02}_{-0.03}$	0.15 ± 0.01	-	0.95	94	0.19 ± 0.02	$540.27/480 = 1.12$
LMC X-3									
1	1.08 ± 0.01	$16.18^{+0.97}_{-0.90}$	3.60 ± 0.09	0.01^{\ddagger}	-	0.65	97	0.19 ± 0.02	$466.08/403 = 1.16$
2	1.10 ± 0.01	$18.24^{+0.57}_{-0.55}$	-	-	$8.29^{+0.30}_{-0.29}$	0.76	97	0.17 ± 0.02	$503.81/393 = 1.28$
3	0.99 ± 0.01	$21.04^{+1.24}_{-0.60}$	-	-	8.16 ± 0.03	0.52	96	0.14 ± 0.02	$430.30/417 = 1.03$
4	1.00 ± 0.02	$18.19^{+2.25}_{-2.95}$	$2.78^{+0.21}_{-0.18}$	0.01^{\ddagger}	-	0.53	96	0.17 ± 0.05	$326.11/318 = 1.03$
5	1.09 ± 0.01	$18.34^{+0.56}_{-0.55}$	-	-	$7.90^{+0.35}_{-0.36}$	0.74	98	0.17 ± 0.01	$529.48/425 = 1.24$
6	1.11 ± 0.01	$20.81^{+1.49}_{-1.71}$	-	-	$8.20^{+1.14}_{-0.69}$	0.93	99	0.18 ± 0.04	$460.08/452 = 1.02$
7	1.13 ± 0.01	$20.16^{+0.52}_{-0.77}$	-	-	$7.99^{+0.10}_{-0.13}$	0.98	98	0.18 ± 0.01	$595.93/453 = 1.31$
8	$1.13^{+0.01}_{-0.02}$	$21.35^{+1.30}_{-0.79}$	-	-	$7.57^{+0.44}_{-0.58}$	1.02	96	0.18 ± 0.01	$535.65/447 = 1.20$
9	1.03 ± 0.01	$17.18^{+0.97}_{-0.86}$	-	-	6.79 ± 0.07	0.53	100 [†]	0.10 ± 0.03	$669.09/480 = 1.39$

* - includes a high energy cut off at 6.29 keV (see section 4.2.1 for details).

† - only disc contribution.

‡ - error is insignificant.

spin parameter is found to be varying from $0.82^{+0.10}_{-0.02}$ – $0.92^{+0.03}_{-0.04}$. During the nine observation epochs of LMC X-3, we find the source mass to be varying from $5.35^{+0.34}_{-0.35} M_{\odot}$ to $6.22^{+0.48}_{-1.74} M_{\odot}$. The value of spin is estimated to be in the range of 0.22 ± 0.02 – 0.41 ± 0.02 . The model fitted parameters along-with the values of spin and mass are tabulated in Table 4. In order to get a better estimation of error of the mass and spin parameters, we have performed Markov Chain Monte Carlo (MCMC) chain simulation using Goodman-Weare algorithm (Goodman & Weare 2010). This is incorporated using *XSpec* where the *walkers* parameter is set to 32, initial chain length is taken to be 15,000 with a burn length of 5,000. In Figure 5, we show the contour plots of mass versus spin values and their probability distributions for the Epoch-4 and Epoch-7 observations of LMC X-1 and LMC X-3 respectively. This is plotted by adapting the MCMC Hammer algorithm (Foreman-Mackey et al. 2013). The contours are plotted for the 68% and 90% confidence intervals (see also Sreehari et al. 2020), showing the range of spin and mass values.

5 DISCUSSION AND CONCLUSIONS

In this paper, we have studied the broadband spectral and temporal variability of the BH sources LMC X-1 and LMC X-3 using *AstroSat* archival and legacy data. For LMC X-1 we study the source characteristics during five different observation epochs and for LMC X-3 nine observations have been looked into; all spanning over the *AstroSat* era of ~ 4.5 years.

We studied the evolution of source light curve and hardness ratio over long term and short term duration using *MAXI* and *AstroSat-LAXPC* observations. The fractional variance has been estimated to be around 24.9% for LMC X-1, from the long term *MAXI* light curve. Whereas in case of LMC X-3, the long term light curve exhibits a high value of variance $\sim 53\%$ over 4.5 years. Applying the same procedure as discussed in section 3.1 to the entire *RXTE*-

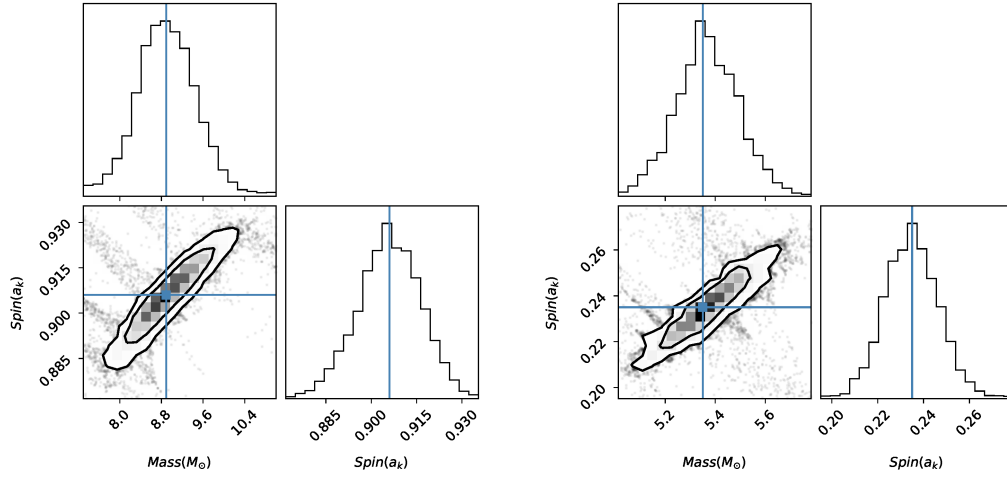


Figure 5. Contour plot of mass versus spin plotted for Epoch-4 of LMC X-1 (left plot) and Epoch-7 of LMC X-3 (right plot) adapting MCMC Hammer algorithm. The corner plot shows the contour of mass versus spin with 68 and 90% confidence. Top panel shows the probability distribution of mass and the right panel shows the distribution of spin.

Table 4. Best-fit parameters obtained by fitting Model-2 for continuum-fitting of broadband energy spectra. The value of d is frozen to 48.1 kpc, while i is considered as $36.38 \pm 1.92^\circ$ for LMC X-1 and $69.24 \pm 0.72^\circ$ for LMC X-3 (see section 1). BH mass M_{BH} is constrained to be in the range of $7.0 - 12.0M_\odot$ and $5.0 - 8.0M_\odot$ for LMC X-1 and LMC X-3 respectively. Spectral hardening factor of 1.55 and 1.7 has been considered for this fitting of LMC X-1 and LMC X-3 respectively. Parameter \dot{M} is the accretion rate in units of 10^{18} g/s, Γ is the photon index, $FracScat$ is the scattering fraction, a represents the source spin and M_{BH} is the mass in units of M_\odot . Error of all the parameters are estimated at 90% confidence.

LMC X-1						
Epoch	\dot{M} $\times 10^{18}(\text{g/s})$	Γ^*	$FracScat^*$	a	M_{BH} (M_\odot)	χ^2/dof
1	$1.60^{+0.01}_{-0.16}$	$4.46^{+0.24}_{-0.31}$	$0.20^{+0.03}_{-0.02}$	$0.86^{+0.08}_{-0.01}$	$9.39^{+0.50}_{-0.46}$	$744.50/529 = 1.40$
2	$2.16^{+0.39}_{-0.17}$	$2.61^{+0.15}_{-0.19}$	$0.13^{+0.01}_{-0.02}$	$0.82^{+0.10}_{-0.02}$	$10.00^{+0.52}_{-1.22}$	$682.18/417 = 1.50$
3	$1.24^{+0.10}_{-0.11}$	$3.04^{+1.13}_{-0.78}$	$0.03^{+0.03}_{-0.01}$	0.90 ± 0.03	$7.64^{+0.99}_{-1.22}$	$631.94/510 = 1.24$
4	$1.48^{+0.24}_{-0.15}$	$3.31^{+0.57}_{-0.36}$	$0.09^{+0.03}_{-0.02}$	$0.91^{+0.03}_{-0.07}$	$8.92^{+0.22}_{-1.13}$	$397.53/338 = 1.18$
5	$1.29^{+0.12}_{-0.13}$	$4.50^{+0.03}_{-1.28}$	$0.09^{+0.04}_{-0.05}$	$0.92^{+0.03}_{-0.04}$	$7.99^{+0.76}_{-0.44}$	$545.63/490 = 1.11$
LMC X-3						
1	$2.88^{+0.07}_{-0.06}$	-	-	$0.30^{+0.01}_{-0.03}$	$5.89^{+0.17}_{-0.25}$	$494.27/403 = 1.22$
2	3.39 ± 0.11	-	-	0.30 ± 0.02	$5.82^{+0.22}_{-0.18}$	$472.38/394 = 1.20$
3	$2.66^{+0.07}_{-0.06}$	-	-	$0.30^{+0.03}_{-0.01}$	$5.70^{+0.15}_{-0.22}$	$424.05/419 = 1.01$
4	$2.51^{+0.89}_{-0.13}$	-	-	$0.38^{+0.01}_{-0.04}$	$6.22^{+0.48}_{-1.74}$	$316.21/314 = 1.01$
5	$2.97^{+0.11}_{-0.05}$	-	-	$0.39^{+0.12}_{-0.01}$	$6.22^{+0.18}_{-0.17}$	$572.34/423 = 1.35$
6	$4.03^{+0.17}_{-0.14}$	-	-	0.22 ± 0.03	$5.35^{+0.34}_{-0.35}$	$567.15/452 = 1.25$
7	$3.98^{+0.04}_{-0.02}$	-	-	$0.23^{+0.02}_{-0.01}$	$5.35^{+0.20}_{-0.17}$	$536.32/453 = 1.18$
8	$3.97^{+0.16}_{-0.04}$	-	-	0.29 ± 0.02	$5.29^{+0.28}_{-0.16}$	$600.85/447 = 1.34$
9	$2.02^{+0.09}_{-0.06}$	-	-	0.41 ± 0.02	$5.50^{+0.10}_{-0.07}$	$663.31/480 = 1.38$

* *simpl* model required only for those epochs with significant data > 10 keV (see text for details).

† Frozen

‡ Upper limit

ASM light curve¹⁰ for ~ 15 years in 3 – 12 keV band, we obtain the fractional variance as 34% and 76% for LMC X-1 and LMC X-3 respectively. On comparing this with the results we obtained using *MAXI* data, it agrees that variability of LMC X-1 on large time scale is less whereas that of LMC X-3 is very high.

We note that the short term *LAXPC* light curve variability varies from 7.41% to 15.89% for LMC X-1, while it is in the range 9.7% - 23.9% for LMC X-3 (see Table 2). We observe that on long time-scales the value of HR remains constant for LMC X-1, while

it has a significant variation with a periodic pattern for LMC X-3. From Figure 2 we find that LMC X-1 does not show any periodic nature in its light curve, while LMC X-3 does. The light curve periodicity of LMC X-3 during the initial 700 days is $\sim 100 - 200$ days, which is similar to that reported earlier by Cowley et al. 1991; Nowak et al. 2001; Smale & Boyd 2012. However, since MJD 58100 the variability pattern becomes random and do not follow the periodic nature (see right panel of Figure 2).

We explored the temporal properties of the source by generating the PDS. For all epochs of LMC X-1 and LMC X-3, the PDS shows only weak power-law nature as evident from the left and right panels of Figure 3. The fractional rms amplitude varies in

¹⁰ <http://xte.mit.edu/asmlc/One-Day.html>

between 9% and 16.7% for LMC X-1 and 7.16% – 10.9% for LMC X-3 (see Table 2). We also did not observe any QPOs during the different epochs, even though previous publications have reported presence of mHz QPOs in LMC X-1 (Alam et al. 2014) and LMC X-3 (Boyd et al. 2000) in LHS. The weak power-law nature of the PDS, fractional rms and absence of QPOs support the fact that the sources have characteristics of a soft state. Thus from both spectral and temporal characteristics, we understand that the sources remain in a thermal emission dominated spectral state.

The spectral fits performed for the broadband *AstroSat* observations of the sources are very well described by a thermal disc emission, with presence of occasional steep power-law of photon index $\sim 2.4 - 3.2$ (see Figure 4 and Table 3). From Table 3, we find that the disc temperature remains around 1 keV and the fractional disc flux contribution is observed to change between 79% and 94% during the different epochs for LMC X-1. We also find that the hardness ratio varies from 0.16 to 0.34 during the epochs. This suggests that source spectra are dominated by thermal disc component during all the five epochs. For LMC X-3, we observe that the disc temperature is ~ 1 keV, fractional disc flux is $> 96\%$ and HR is 0.10–0.19 (Table 3) during the different epochs. These variations in the spectral parameters indicate that the source LMC X-3 occupied a disc dominated high soft state during the *AstroSat* observations. The values of disc parameters obtained are consistent with that obtained by the *BeppoSAX* (Treves et al. 2000; Haardt et al. 2001) and *RXTE* observations (Nowak et al. 2001). The bolometric luminosity estimated of $0.07 - 0.10 L_{Edd}$ and $0.06 - 0.14 L_{Edd}$ suggests that the sources LMC X-1 and LMC X-3 are emitting in sub-Eddington. We also did attempt to find the ‘true’ radius of the accretion disc following Kubota et al. 1998 and got a value of 29.65 – 39.17 km for LMC X-1 and 32.40 – 37.2 km for LMC X-3, which are within ± 3 km of the mean value. We understand that the radius varies over a long time period for both sources. It has to be noted that these estimations of radius do not follow in sync¹¹ with the source mass estimated (see section 4.3) and reported earlier (Orosz et al. 2009, 2014). We did not observe any strong Fe K_{α} line in both sources. But a reflection edge was seen which possibly has a minimal contribution to the total unabsorbed flux.

Further, we attempt to constrain the source parameters: mass and spin. Since there were no Fe K_{α} emission line detected, we have chosen the continuum fitting method over the entire broadband *AstroSat* energy range considered. By using the *kerrd* model, we were able to get acceptable spectral fit parameters (mass of $12.64 - 13.00 M_{\odot}$) during the different epochs of LMC X-1 but not for any of the observations of LMC X-3. This suggests that the source LMC X-1 belongs to the category of extremely rotating BHs, while LMC X-3 is a weakly rotating source. Using the *kerrbb* and *simpl* model combination, we were able to constrain both sources’ mass, spin and accretion rate. In order to get better estimations on errors of these parameters, we have performed MCMC chain simulation using Goodman-Weare algorithm (Goodman & Weare 2010) within *XSpec*. Errors estimated with 90% confidence using this chain yielded a better estimation. We cross-check these error values with the error estimation using MCMC hammer algorithm (Figure 5). We find that the mass for LMC X-1 to be in the range of $7.64^{+0.99}_{-0.25} M_{\odot}$ to $10.00^{+0.52}_{-1.22} M_{\odot}$ and for LMC X-3 it is $5.35^{+0.34}_{-0.34} M_{\odot}$.

¹¹ Considering $R_{ISCO} = 9$ km for a non-rotating BH of mass $1M_{\odot}$ and 3 km for an extremely rotating BH with same mass, where R_{ISCO} is the radius of innermost stable circular orbit (Shapiro & Teukolsky 1983; Remillard & McClintock 2006)

M_{\odot} to $6.22^{+0.48}_{-1.74} M_{\odot}$. All these estimates are in close agreement with the dynamical mass estimate of $10.91 \pm 1.41 M_{\odot}$ and $6.98 \pm 0.56 M_{\odot}$ reported by (Orosz et al. 2009, 2014) for LMC X-1 and LMC X-3 respectively. Similarly, the spin estimate of $0.82^{+0.10}_{-0.02} - 0.92^{+0.04}_{-0.05}$ for LMC X-1 agrees with the previous report by Gou et al. 2009; Tripathi et al. 2020. Mudambi et al. (2020) has recently reported a spin value of 0.93 by analyzing the first two *AstroSat* observations of LMC X-1, but by considering only the Galactic abundance and a higher spectral hardening factor (1.7). For LMC X-3, the spin estimated is $0.22 \pm 0.03 - 0.41 \pm 0.02$ within 90% confidence interval (see section 4.3, Figure 5 and Table 4), which is better constrained w.r.t. that already reported ($0.25^{+0.20}_{-0.29}$; Steiner et al. 2010). We also check the rotating nature of the sources following Makishima et al. 2000, which expresses the source mass as $M_x = R_{in}/8.86\alpha$. Here, α is the positive parameter which has a value of 1 for non-rotating BHs and 1/6 for BHs with extreme rotation. Considering the value of the ‘true’ radius of the accretion disc and the average source mass estimated (see section 4.2.1, 4.2.2, 4.3), we find the value of α to be 0.37 – 0.50 for LMC X-1 and 0.63 – 0.73 for LMC X-3. These estimates of α suggest that the source LMC X-1 probably is a maximally rotating ‘hole’, which is also supported by the spin estimation of 0.82 – 0.92. Also, the value of α being close to 1 for LMC X-3 suggests that the compact object could be a weakly rotating BH. This fact is consistent with the estimate of spin using continuum fitting method as 0.22 – 0.41.

LMC X-1 and LMC X-3 are peculiar when compared to other persistent BH-XRBs in term of the spectral behavior. Based on the study of spectral and temporal evolution of the sources using *AstroSat* observations discussed in this paper, we observe the sources remain in a thermally dominated state over a long duration. We observe that LMC X-3 exists in a HSS during all the *AstroSat* observations conducted till date. Previous publications have mentioned a state transition to LHS, which probably suggest frequent monitoring observations of the source are required to probe the accretion dynamics. Similar kind of spectral state transitions over long time scales have been observed for other persistent sources like Cyg X-1 (Gierliński et al. 1999), GRS 1758-258 and 1E 1740.7-2942 (Main et al. 1999) using *RXTE* observations.

Based on the spectral and temporal studies for the sources LMC X-1 and LMC X-3 using *AstroSat* observations, we summarize our results with the following conclusions:

- The study of *MAXI* light curves over a duration of 4.5 years show that LMC X-1 has a long term fractional variability of 25%, while LMC X-3 has a higher variability of 53%.
- Long term light curve periodicity of $\sim 100 - 200$ days seen for LMC X-3 during the initial 700 days, while the variability pattern becomes random later without having any periodic nature.
- LMC X-1 is moderately variable from 7.4% – 16% over short time scale, while LMC X-3 has variability ranging from 9.7% – 24% during the different observation epochs.
- The spectral characteristics suggest the sources have a thermal disc dominated energy spectra.
- The weak power-law nature of PDS and evolution of fractional rms amplitude with the absence of low-frequency QPOs supports that sources remained in the thermally dominated soft state.
- We constrain the source mass in the range of $7.64 - 10.00 M_{\odot}$ for LMC X-1, and $5.35 - 6.22 M_{\odot}$ for LMC X-3, which are in close agreement with that already reported.
- The spin parameter is estimated to be 0.82 – 0.92 for LMC X-1 and is consistent with previous publications. In case of LMC

X-3, we could obtain a better constrain of the spin as 0.22 – 0.41 in contrast with that reported earlier.

ACKNOWLEDGEMENTS

The authors thank the anonymous reviewer for valuable suggestions which have helped in improving this manuscript. We acknowledge the financial support of Indian Space Research Organization (ISRO) under *AstroSat* archival data utilization program Sanction order No. DS-2B-13013(2)/13/2019-Sec.2. This publication uses data from the *AstroSat* mission of the ISRO archived at the Indian Space Science Data Centre (ISSDC). This work has been performed utilizing the calibration databases and auxiliary analysis tools developed, maintained and distributed by *AstroSat-SXT* team with members from various institutions in India and abroad. This research has made use of *MAXI* data provided by RIKEN, JAXA and the *MAXI* team. Also this research made use of software provided by the High Energy Astrophysics Science Archive Research Center (HEASARC) and NASA's Astrophysics Data System Bibliographic Services. VKA, AN also thank GH, SAG, DD, PDMSA and Director, URSC for encouragement and continuous support to carry out this research.

Facilities: *AstroSat*, *MAXI*.

DATA AVAILABILITY

The data used for analysis in this article are available in *AstroSat*-ISSDC website (https://astrobrowse.issdc.gov.in/astro_archive/archive/Home.jsp) and *MAXI* website (<http://maxi.riken.jp/top/index.html>).

References

- Agrawal P. C., 2001, in Inoue H., Kunieda H., eds, *Astronomical Society of the Pacific Conference Series Vol. 251, New Century of X-ray Astronomy*. p. 512
- Agrawal V. K., Nandi A., Girish V., Ramadevi M. C., 2018, *MNRAS*, **477**, 5437
- Alam M. S., Dewangan G. C., Belloni T., Mukherjee D., Jhingan S., 2014, *MNRAS*, **445**, 4259
- Aneasha U., Mandal S., Sreehari H., 2019, *MNRAS*, **486**, 2705
- Antia H. M., et al., 2017, *ApJS*, **231**, 10
- Arnaud K. A., 1996, in Jacoby G. H., Barnes J., eds, *Astronomical Society of the Pacific Conference Series Vol. 101, Astronomical Data Analysis Software and Systems V*. p. 17
- Baby B. E., Agrawal V. K., C R. M., Katoch T., Antia H. M., Mandal S., Nandi A., 2020, *MNRAS*,
- Belloni T., 2005, in Burderi L., Antonelli L. A., D'Antona F., di Salvo T., Israel G. L., Piersanti L., Tornambè A., Straniero O., eds, *American Institute of Physics Conference Series Vol. 797, Interacting Binaries: Accretion, Evolution, and Outcomes*. pp 197–204 ([arXiv:astro-ph/0504185](https://arxiv.org/abs/astro-ph/0504185)), doi:10.1063/1.2130233
- Belloni T., Hasinger G., 1990, *A&A*, **230**, 103
- Belloni T. M., Motta S. E., Muñoz-Darias T., 2011, *Bulletin of the Astronomical Society of India*, **39**, 409
- Bevington P. R., Robinson D. K., 2003, *Data reduction and error analysis for the physical sciences*
- Boller T., et al., 2002, *MNRAS*, **329**, L1
- Boyd P. T., Smale A. P., Homan J., Jonker P. G., van der Klis M., Kuulkers E., 2000, *ApJ*, **542**, L127
- Casella P., Belloni T., Stella L., 2005, *ApJ*, **629**, 403
- Chakrabarti S., Titarchuk L. G., 1995, *ApJ*, **455**, 623
- Chen X., Taam R. E., 1996, *ApJ*, **466**, 404
- Chen W., Shrader C. R., Livio M., 1997, *ApJ*, **491**, 312
- Corral-Santana J. M., Casares J., Muñoz-Darias T., Bauer F. E., Martínez-Pais I. G., Russell D. M., 2016, *A&A*, **587**, A61
- Cowley A. P., et al., 1991, *ApJ*, **381**, 526
- Cowley A. P., Schmidtke P. C., Anderson A. L., McGrath T. K., 1995, *PASP*, **107**, 145
- Ebisawa K., Mitsuda K., Inoue H., 1989, *PASJ*, **41**, 519
- Ebisawa K., Makino F., Mitsuda K., Belloni T., Cowley A. P., Schmidtke P. C., Treves A., 1993, *ApJ*, **403**, 684
- Fabian A. C., Vaughan S., 2003, *MNRAS*, **340**, L28
- Fabian A. C., et al., 2002, *MNRAS*, **335**, L1
- Foreman-Mackey D., Hogg D. W., Lang D., Goodman J., 2013, *PASP*, **125**, 306
- Gierliński M., Zdziarski A. A., Poutanen J., Coppi P. S., Ebisawa K., Johnson W. N., 1999, *MNRAS*, **309**, 496
- Goodman J., Weare J., 2010, *Communications in Applied Mathematics and Computational Science*, **5**, 65
- Gou L., et al., 2009, *ApJ*, **701**, 1076
- Haardt F., et al., 2001, *ApJS*, **133**, 187
- Hanke M., Wilms J., Nowak M. A., Barragán L., Schulz N. S., 2010, *A&A*, **509**, L8
- Homan J., Wijnands R., van der Klis M., Belloni T., van Paradijs J., Klein-Wolt M., Fender R., Méndez M., 2001, *ApJS*, **132**, 377
- Katoch T., Blessy E. B., Nandi A., Agrawal V. K., Antia H. M., Mukerjee M., 2020
- Kubota A., Tanaka Y., Makishima K., Ueda Y., Dotani T., Inoue H., Yamaoka K., 1998, *PASJ*, **50**, 667
- Li L.-X., Zimmerman E. R., Narayan R., McClintock J. E., 2005, *ApJS*, **157**, 335
- Main D. S., Smith D. M., Heindl W. A., Swank J., Leventhal M., Mirabel I. F., Rodríguez L. F., 1999, *ApJ*, **525**, 901
- Makishima K., et al., 2000, *ApJ*, **535**, 632
- Mark H., Price R., Rodrigues R., Seward F. D., Swift C. D., 1969, *ApJ*, **155**, L143
- McClintock J. E., Remillard R. A., 1986, *ApJ*, **308**, 110
- McClintock J. E., Shafee R., Narayan R., Remillard R. A., Davis S. W., Li L.-X., 2006, *ApJ*, **652**, 518
- McClintock J. E., et al., 2011, *Classical and Quantum Gravity*, **28**, 114009
- McClintock J. E., Narayan R., Steiner J. F., 2014, *Space Sci. Rev.*, **183**, 295
- Mudambi S. P., Rao A., Gudennavar S. B., Misra R., Bubbly S. G., 2020, *MNRAS*, **498**, 4404
- Nandi A., Debnath D., Mandal S., Chakrabarti S. K., 2012, *A&A*, **542**, A56
- Nandi A., et al., 2018, *Ap&SS*, **363**, 90
- Nowak M. A., 1995, *PASP*, **107**, 1207
- Nowak M. A., Wilms J., Heindl W. A., Pottschmidt K., Dove J. B., Begelman M. C., 2001, *MNRAS*, **320**, 316
- Orosz J. A., et al., 2009, *ApJ*, **697**, 573
- Orosz J. A., Steiner J. F., McClintock J. E., Buxton M. M., Bailyn C. D., Steeghs D., Guberman A., Torres M. A. P., 2014, *ApJ*, **794**, 154
- Radhika D., Nandi A., 2014, *Advances in Space Research*, **54**, 1678
- Radhika D., Nandi A., Agrawal V. K., Seetha S., 2016a, *MNRAS*, **460**, 4403
- Radhika D., Nandi A., Agrawal V. K., Mandal S., 2016b, *MNRAS*, **462**, 1834
- Radhika D., Sreehari H., Nandi A., Iyer N., Mandal S., 2018, *Ap&SS*, **363**, 189
- Remillard R. A., McClintock J. E., 2006, *ARA&A*, **44**, 49
- Schmidtke P. C., Ponder A. L., Cowley A. P., 1999, *AJ*, **117**, 1292
- Shafee R., McClintock J. E., Narayan R., Davis S. W., Li L.-X., Remillard R. A., 2006, *ApJ*, **636**, L113
- Shakura N. I., Sunyaev R. A., 1973, *A&A*, **500**, 33
- Shapiro S. L., 1973, *ApJ*, **180**, 531
- Shapiro S. L., Teukolsky S. A., 1983, *Black holes, white dwarfs, and neutron stars: the physics of compact objects*
- Singh K. P., et al., 2017, *Journal of Astrophysics and Astronomy*, **38**, 29
- Smale A. P., Boyd P. T., 2012, *ApJ*, **756**, 146
- Soria R., Wu K., Page M. J., Sakellou I., 2001, *A&A*, **365**, L273
- Sreehari H., Nandi A., Radhika D., Iyer N., Mandal S., 2018, *Journal of Astrophysics and Astronomy*, **39**, 5

- Sreehari H., Ravishankar B. T., Iyer N., Agrawal V. K., Katoch T. B., Mandal S., Nandi A., 2019, *MNRAS*, **487**, 928
- Sreehari H., Nandi A., Das S., Agrawal V. K., Mandal S., Ramadevi M. C., Katoch T., 2020, *MNRAS*, **499**, 5891
- Steiner J. F., Narayan R., McClintock J. E., Ebisawa K., 2009, *PASP*, **121**, 1279
- Steiner J. F., McClintock J. E., Remillard R. A., Gou L., Yamada S., Narayan R., 2010, *ApJ*, **718**, L117
- Steiner J. F., McClintock J. E., Orosz J. A., Remillard R. A., Bailyn C. D., Kolehmainen M., Straub O., 2014, *ApJ*, **793**, L29
- Tanaka Y., Lewin W. H. G., 1995, X-ray Binaries, pp 126–174
- Tanaka Y., Shibazaki N., 1996, *ARA&A*, **34**, 607
- Tetarenko B. E., Sivakoff G. R., Heinke C. O., Gladstone J. C., 2016, *ApJS*, **222**, 15
- Torpin T. J., Boyd P. T., Smale A. P., Valencic L. A., 2017, *ApJ*, **849**, 32
- Trèves A., Belloni T., Chiappetti L., Maraschi L., Stella L., Tanzi E. G., van der Klis M., 1988, *ApJ*, **325**, 119
- Trèves A., et al., 2000, *Advances in Space Research*, **25**, 437
- Tripathi A., et al., 2020, *ApJ*, **897**, 84
- Tsunemi H., Kitamoto S., Okamura S., Roussel-Dupre D., 1989, *ApJ*, **337**, L81
- Vaughan S., Reeves J., Warwick R., Edelson R., 1999, *MNRAS*, **309**, 113
- Vaughan S., Edelson R., Warwick R. S., Uttley P., 2003, *MNRAS*, **345**, 1271
- Wilms J., Allen A., McCray R., 2000, *ApJ*, **542**, 914
- Wilms J., Nowak M. A., Pottschmidt K., Heindl W. A., Dove J. B., Begelman M. C., 2001, *MNRAS*, **320**, 327
- Yadav J. S., et al., 2016, Large Area X-ray Proportional Counter (LAXPC) instrument onboard ASTROSAT, p. 99051D, doi:10.1117/12.2231857
- Zdziarski A. A., Poutanen J., Paciesas W. S., Wen L., 2002, *ApJ*, **578**, 357
- Zhang S. N., Cui W., Harmon B. A., Paciesas W. S., Remillard R. E., van Paradijs J., 1997a, *ApJ*, **477**, L95
- Zhang S. N., Cui W., Chen W., 1997b, *ApJ*, **482**, L155
- Życki P. T., Done C., Smith D. A., 1999, *MNRAS*, **309**, 561

This paper has been typeset from a $\text{\TeX}/\text{\LaTeX}$ file prepared by the author.